IEEE Access
Multidisciplinary | Rapid Review | Open Access Journal

Received November 16, 2021, accepted December 17, 2021, date of publication January 6, 2022, date of current version January 14, 2022.

Digital Object Identifier 10.1109/ACCESS.2022.3140760

Stabilized Controller for Jet Actuated Cantilevered Pipe Using Damping Effect of an Internal Flowing Fluid

YUICHI AMBE[1], (Member, IEEE), YU YAMAUCHI[2], (Graduate Student Member, IEEE), MASASHI KONYO[1,2], (Member, IEEE), KENJIRO TADAKUMA[1], (Member, IEEE), AND SATOSHI TADOKORO[1,2], (Fellow, IEEE)

[1]Tough Cyberphysical AI Research Center, Tohoku University, Sendai 9808579, Japan
[2]Graduate School of Information Sciences, Tohoku University, Sendai 9808579, Japan

Corresponding author: Yuichi Ambe (ambe@rm.is.tohoku.ac.jp)

This work was supported in part by the Research Grant from the Fluid Power Technology Promotion Foundation, and in part by the Japan Society for the Promotion of Science (JSPS) KAKENHI under Grant JP19H00748.

ABSTRACT Fluid jet actuation is a potential actuation technique for continuum robots. It can generate and rapidly control a relatively large force using a small and lightweight structure because a significant amount of energy can be transported through its internal channels. Recently, jet-actuated flying continuum robots have been developed using this advantageous characteristic. However, a challenging issue in controlling the robot is the fluid structure interaction between the flexible body and the internal flowing fluid. This interaction often causes instability in the pipe conveying fluid. In this study, as a first step to address this issue, we propose a stabilized controller (vertical position control) for a jet-actuated two-dimensional cantilevered pipe with a nozzle unit at the tip using the damping effect of the internal flowing fluid and verify the controller with a real robot. Specifically, a model is constructed with the net force of the jets as the control input. A simple controller that can constantly decrease the energy function is proposed by utilizing the damping effect of the flowing fluid. Numerical simulations verify the stability of the system regardless of the flow velocity. In particular, fluid damping mainly suppresses the higher-order mode oscillations. Moreover, the stability of the system can be improved by adjusting the controller gains. We also conduct experiments using an actual robot to verify the simulation results. The vibrations can be damped by the fluid effect, and the stability can be improved using the proposed controller.

INDEX TERMS Continuum robot, fluid jet, cantilevered pipe, fluid structure interaction, stabilized levitation.

I. INTRODUCTION

Fluid jet actuation is one of the potential actuators for continuum robots because it can generate and rapidly control a relatively large force using a small and lightweight structure. The jet-actuated continuum robot uses the reaction forces of the fluid jets to transform the shape. The fluid is delivered through a channel in the body. It can generate a relatively large force with a lightweight and thin body structure because an energy source such as a pump can be located at the root. In particular, a large force can be controlled with a high responsivity if rotating nozzles are used because the jet reaction force can be rotated without any torque when the jet direction is perpendicular to the rotating axis [1]. Therefore, because of these advantages, some studies have proposed fluid jet actuation for continuum robots. For instance, some studies developed a water injection thin continuum robot, with a tip driven by three jets, to investigate nuclear reactors [2], and for rapid investigation of organs [3]. A fluid jet actuator that can be attached to the middle of a hose has also been developed [4]. Furthermore, to explore narrow debris, we developed an active scope camera that can elevate this tip using air injection [5].

Moreover, a flying continuum robot can be realized by mounting multiple nozzle units. We proposed a flying firefighting hose (Dragon Fire Fighter) driven by water

The associate editor coordinating the review of this manuscript and approving it for publication was Hui Xie.

jets [6]–[8]. A similar concept was proposed in [9]. Our goal is to float the hose and directly reach the fire source by controlling the reaction forces of the distributed nozzle units. The nozzle unit consists of multiple rotating nozzles and generates a net force with high responsivity by adjusting the nozzle angles. To date, we have achieved stable levitation and direction switching of 4-m robots by attaching one nozzle unit each on the tip and the middle [8].

A key issue in controlling the jet-actuated flying continuum robot is the fluid structure interaction between the flexible body and the internal flowing fluid. This is because the interaction becomes non-negligible as the body length increases. Generally, when a fluid flows inside an elastic structure, the fluid structure interaction causes a vibration phenomenon. In particular, when a fluid flows in a cantilevered elastic tube with an open end, the system becomes a non-conservative system. A flutter phenomenon, in which the deflection increases while vibrating, occurs when the flow velocity exceeds a specific limit.

However, these interactions have not been considered for jet-actuated continuum robots. This is because the robot is flexible and can be deformed nonlinearly into various shapes in a three-dimensional space, which complicates the interaction with the fluid. In addition, if there are multiple nozzle units, the flow path branches to make the system more complex.

In this study, as a first step, we propose a stabilized controller (vertical position controller) for a jet-actuated two-dimensional cantilevered pipe with a nozzle unit at the tip using the damping effect of the internal flowing fluid, and verify the controller with an actual robot. First, we construct a two-dimensional cantilevered water pipe model with a head nozzle unit considering fluid motion. We assume that the nozzle unit can control the magnitude and direction of the net force by changing the directions of multiple jets. Next, based on the characteristics of the equations of motion, we propose a vertical position controller using the net force as an input. The controller can always decrease the energy function of the system, regardless of the flow velocity, using the damping effect of the flowing fluid. Through numerical simulations, we validate the stability of the controller, which can be improved by using the damping effect of the fluid and tuning the control gains. Furthermore, the validity of the proposed controller is demonstrated through experiments using actual robots.

The contributions of this study are as follows: (1) We propose a stabilized controller for a cantilevered pipe with multiple fluid injections for the first time. The controller can utilize the damping effect of the flowing fluid for stabilization. Although many studies have assessed the stabilization of the pipe, as discussed in the next section, no study has yet proposed a stabilized controller using multiple jets. (2) The validity of the proposed controller is verified through simulations and experiments. Although these results cannot be directly applied to jet-actuated continuum robots owing to the difference in stiffness, they provide significant suggestions and insights for future control strategies of jet-actuated continuum robots. For example, the proposed control strategy, using the damping property of an internal flowing fluid, would be very useful for continuum robots, which are also distributed parameter systems with a limited number of actuators.

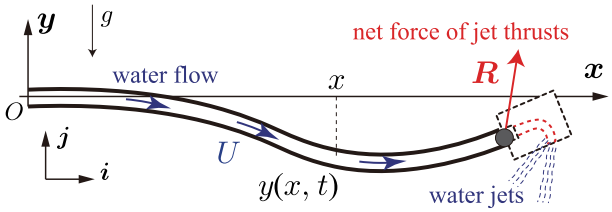

FIGURE 1. Model of a cantilevered pipe conveying fluid using nozzles.

II. RELATED STUDIES

Many studies have investigated the dynamics and instability of the cantilevered pipe conveying fluid [10], [11]. A straight cantilevered pipe, with an open end, loses stability via flutter when the flow velocity increases. Thus far, rich dynamic properties have been investigated by changing various physical parameters. For example, chaotic motions occur by adding an end mass [12], spring supports [13], [14], or motion constraints [15]. In addition, some studies have investigated movements with a large deformation [16], [17], including in three-dimensions [18], with an initially curved tube [19], and with pulsatile flow [20], [21]. In particular, Sugiyama [22] pointed out that the flowing fluid inside a cantilevered pipe contributes to damping the body oscillation in the case of a slow-flowing speed. Our study also utilizes this damping effect. However, our proposed jet controller can ensure a damping effect regardless of the flow speed range.

In terms of the stabilized controller, although many studies have discussed methods to stabilize the cantilever pipe conveying fluid, no study has yet used multiple jets to stabilize the pipe. For example, Doki *et al.* proposed a method to damp vibrations by controlling the tendon mechanism [23]. Pisarski *et al.* proposed a damping method using electromagnetic devices [24]. Several researchers have attached a nonlinear energy sink to the pipe, which dissipates the vibrational energy of the pipe [25]–[27]. Yu *et al.* controlled the tip bending moment using piezoelectric actuators to increase the critical flow velocity [28]. Although Borglund attempted to dampen fluttering by controlling the jet direction using a proportional derivative (PD) controller at the tip [29], no study has yet used multiple jets. We control the magnitude of the net force by controlling multiple jets to stabilize the cantilevered pipe conveying fluid.

III. MODEL OF CANTILEVERED PIPE WITH A NOZZLE UNIT

A. ASSUMPTIONS AND MODEL

Our targeted jet-actuated cantilevered pipe consists of an elastic beam and a nozzle unit, as shown in Fig. 1. The nozzle unit

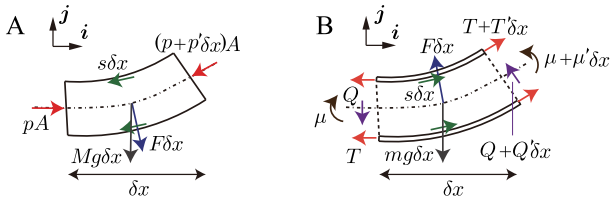

FIGURE 2. Forces and moments applied on elements of A: fluid and B: tube.

can control the net force by adjusting multiple jets' directions. The model was developed under the following assumptions:

(A1) The model consists of a uniform tubular beam of length L on a sagittal plane($O-xy$). The root is fixed at the origin O, and the vertical displacement $y(x,t)$, as a function of the position x and time t, is considered small enough to neglect second-order terms (Euler Bernoulli beam approximation).

(A2) The target fluid is a Newtonian fluid and flows through the uniform channel inside the beam. The flow speed U is constant along the channel. We assume a plug flow, and the pipe friction is sufficiently small.

(A3) The nozzle unit is attached to the tip as the mass point of weight m_n and has multiple direction controllable outlets. It generates a controllable force $\boldsymbol{R}$ (control input of the system) by adjusting these directions.

Assumptions (A1 and A2) are frequently used to investigate the dynamics of a cantilevered pipe conveying water, as in [30]. The physical variables are shown in Fig. 1. The direction of gravity g is the $-y$-axis. The weights of the beam and fluid per unit length are m and M, respectively. $\boldsymbol{i}$ and $\boldsymbol{j}$ represent the unit vectors along the x and y axes, respectively.

The equation of motion (EQM) can be derived using the following three steps: First, we derive the EQM of a cantilevered pipe conveying the fluid (Section III-B). Then, we derive the boundary conditions by considering the reaction forces generated by the nozzle unit (Section III-C). Finally, combining steps one and two, we derive the EQM of the system (Section III-D). Note that the partial derivatives of position x and time t are represented as $[]'$ and $\dot{[]}$, respectively.

B. EQM FOR A CANTILEVERED PIPE CONVEYING FLUID

Here, we derive the EQM for a cantilevered pipe conveying fluid by referring to [30]. For a small element at x (Fig. 2), we derive the EQMs for the fluid and elastic beam parts independently. Subsequently, we integrate them to derive the EQM for the cantilevered pipe with a fluid. The formulation procedure is identical to that in [30], except for the direction of gravity and boundary conditions discussed in Section III-C.

1) EQM FOR FLUID IN THE SMALL ELEMENT

We derive the EQM for the fluid that flows through the small element B with length δx, as shown in Fig. 2A. p represents the relative pressure. The normal and tangential forces applied by the corresponding pipe on the fluid are represented as $F\delta x$ and $s\delta x$, respectively. We set the flow speed and density as $\boldsymbol{V}$ and ρ, respectively.

From the momentum conservation law of the fluid, we derive the following relations, while considering the small deflection approximation (first-order approximation):

$$\iiint_B \rho\dot{\boldsymbol{V}}\,dB + \iint_{S_B} \rho\,(\boldsymbol{n}\cdot\boldsymbol{V})\,\boldsymbol{V}\,dS_B = (-Ap' + Fy' - s)\delta x\boldsymbol{i} + \left[-A(py')' - F - sy' - Mg\right]\delta x\boldsymbol{j} \tag{1}$$

where S_B and $\boldsymbol{n}$ represent the surface of B and its normal vector, respectively. The first and second terms on the left-hand side represent the variation ratio of the momentum in B and loss ratio of the momentum through the channel sections, respectively. The right-hand term represents the force applied to the fluid. The left side of (1) can be transformed using the Gauss theorem and the equation of continuity ($\nabla\cdot\boldsymbol{V}=0$) as

$$\iiint_B \rho\dot{\boldsymbol{V}}\,dB + \iint_{S_B} \rho\,(\boldsymbol{n}\cdot\boldsymbol{V})\,\boldsymbol{V}\,dS_B = \iiint_B \rho\left[\dot{\boldsymbol{V}} + (\boldsymbol{V}\cdot\nabla)\,\boldsymbol{V}\right]dB. \tag{2}$$

Because the internal flow speed relative to the pipe is constant U (assumption (A2)) and the pipe element moves at a speed of $\dot{y}\boldsymbol{j}$; therefore, the flow speed on the inertial frame $\boldsymbol{V}$ can be derived as follows:

$$\boldsymbol{V} = U\left(\boldsymbol{i} + y'\boldsymbol{j}\right) + \dot{y}\boldsymbol{j} \tag{3}$$

Equation (2) can be further transformed as follows by substituting (3) into (2) and using the expressions $\dot{U}=0$, $\rho A = M$ under the small deflection approximation.

$$\iiint_B \rho\left[\dot{\boldsymbol{V}} + (\boldsymbol{V}\cdot\nabla)\,\boldsymbol{V}\right]dB = M\left(\frac{\partial}{\partial t} + U\frac{\partial}{\partial x}\right)^2 y\delta x\boldsymbol{j} \tag{4}$$

By substituting (2) and (4) into (1), we derive the following EQM of the fluid in the pipe:

$$0 = -Ap' + Fy' - s \tag{5}$$

$$M\ddot{y} + 2MU\dot{y}' + MU^2y'' = -A(py')' - F - sy' - Mg \tag{6}$$

Equation (5) represents the equilibrium of forces in the x direction (forces applied by the pressure, pipe, and gravity). Equation (6) represents the equation of motion in the y direction. The three terms on the left-hand side represent the acceleration, Coriolis term, and y element of the axis force MU^2 applied by the fluid inflow and outflow. The right-hand terms represent the y elements of the forces applied by the pressure, pipe, and gravity. Note that the formulations are identical to those in [30], except for the direction of gravity.

2) EQM FOR PIPE OF SMALL ELEMENT

The EQM for the beam (pipe) is derived by considering a small element with length δx, as shown in Fig. 2B. T is the longitudinal tension, Q is the shear force, and μ is the bending moment. The normal and tangential forces applied by the corresponding fluid to the pipe are represented as $F\delta x$

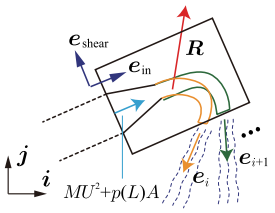

FIGURE 3. Forces applied on a nozzle unit.

and $s\delta x$, respectively. The EQM in the $\boldsymbol{i}$ and $\boldsymbol{j}$ directions can be written as follows by ignoring the deformation along the longitudinal axis:

$$0 = T' - Fy' + s \tag{7}$$

$$m\ddot{y} = Q' + (Ty')' + F + sy' - mg \tag{8}$$

where $Q = -\mu' = -(E^*(\partial/\partial t) + E)Iy'''$, E is the Young's modulus, I is the moment of inertia, and E^* represents the viscoelastic coefficient (Kelvin–Voigt type). Note that the formulations are identical to those in [30], except for the direction of gravity.

3) EQM FOR CANTILEVERED PIPE CONVEYING FLUID

We can derive the EQM for the cantilevered pipe conveying fluid by integrating (6) and (8):

$$(E^*\frac{\partial}{\partial t} + E)Iy'''' - \left[(T - pA)\, y'\right]' + (M + m)\ddot{y} + 2MU\dot{y}' + MU^2y'' + (M + m)g = 0 \tag{9}$$

Moreover, the following condition is derived using (5) and (7):

$$(T - pA)' = 0 \tag{10}$$

This equation determines the term $T - pA$ of (9) by using the boundary condition $p(L)$, $T(L)$ as follows:

$$T - pA = T(L) - p(L)A \tag{11}$$

C. BOUNDARY CONDITION

The nozzle unit can control the magnitude and direction of the net force by adjusting the directions of multiple jets, as shown in Fig. 3. The unit vectors parallel and normal to the nozzle inlet are defined as $\boldsymbol{e}_{in}$ and $\boldsymbol{e}_{shear}$, respectively. Multiple rotating nozzles are attached to the unit, and each nozzle outlet generates a reaction force $\boldsymbol{r}_i = -\rho A_i U_i^2 \boldsymbol{e}_i$, where $\boldsymbol{e}_i$, U_i, and A_i represent the unit vector of the jet direction, outlet flow velocity, and outlet section, respectively. The net force applied to the nozzle unit considering the pressure and momentum gain at the inlet of the nozzle unit can be written as follows:

$$\boldsymbol{F}_n = \boldsymbol{R} + \left[MU^2 + p(L)A\right]\boldsymbol{e}_{in} \tag{12}$$

where $\boldsymbol{R} = \sum \boldsymbol{r}_i$. Note that we ignore the rotational moment of the nozzle unit because the outlets and inlet are in close distance.

Because the nozzle unit and pipe are connected, the tension applied to the tip of pipe $T(L)$ is determined by the $\boldsymbol{e}_{in}$ element of the generated force on the nozzle unit:

$$T(L) = R_i + MU^2 + p(L)A \tag{13}$$

where $R_i = \boldsymbol{R} \cdot \boldsymbol{e}_{in}$. By substituting this equation into (11), we obtain:

$$T - pA = R_i + MU^2 \tag{14}$$

The boundary condition of the $\boldsymbol{e}_{shear}$ element of the force can be written as:

$$Q(L) = R_s \tag{15}$$

where $R_s = \boldsymbol{R} \cdot \boldsymbol{e}_{shear}$. Equations (14) and (15) are different from those in previous studies, such as [30].

In addition, the boundary conditions for the moment at the tip, and for the position and posture at the fixed root, are

$$\mu(L) = 0,\ y(0) = 0,\ y'(0) = 0. \tag{16}$$

D. EQM FOR CANTILEVERED PIPE WITH NOZZLE UNIT

We represent the mass of the pipe per unit length as $m + m_n\delta(L - x)$ because the weight of the nozzle unit is m_n. In the above discussion, we derive the following EQM by substituting (11)(14) into (9).

$$EIy'''' + E^*I\dot{y}'''' + \hat{M}\ddot{y} + \hat{M}g + 2MU\dot{y}' - \left(R_i y'\right)' = 0 \tag{17}$$

where $\hat{M} = M + m + m_n\delta(L - x)$. The boundary conditions are derived using (15)(16) as follows:

$$y(0) = 0, \quad y'(0) = 0,$$
$$(E^*\frac{\partial}{\partial t} + E)Iy''(L) = 0, \quad (E^*\frac{\partial}{\partial t} + E)Iy'''(L) = -R_s, \tag{18}$$

In (17), the first four terms represent the motion of the Euler–Bernoulli beam under gravity. The fifth and sixth terms represent the Coriolis term of the fluid and the effect of the $\boldsymbol{e}_{in}$ element of $\boldsymbol{R}$, respectively. In (18), the first three terms are the ordinal constraints for the cantilevered beam. The fourth term represents the $\boldsymbol{e}_{shear}$ element of $\boldsymbol{R}$. The pressure p and longitudinal forces between the pipe and fluid s do not affect the motion in this model as [11]. Furthermore, the tip nozzle eliminates the momentum effect that flows along the pipe MU^2 and is different from the standard models [11]. We set the control inputs in this study as the net forces R_i and R_s.

In addition, we derive another representation of the EQM, with boundary conditions identical to the Euler–Bernoulli beam for simulation, by using the Dirac delta function.

$$EIy'''' + E^*I\dot{y}'''' + \hat{M}\ddot{y} + \hat{M}g + 2MU\dot{y}' - \frac{\partial}{\partial x}\left(R_i y'\right) - R_s\delta(x - L) = 0. \tag{19}$$

where the boundary conditions are

$$y(0) = 0, \quad y'(0) = 0,$$
$$(E^*\frac{\partial}{\partial t} + E)Iy''(L) = 0, \quad (E^*\frac{\partial}{\partial t} + E)Iy'''(L) = 0 \tag{20}$$

IV. PROPOSED CONTROLLER

We propose a controller based on the energy dissipation feature of the internal flow [22]. First, we explain the time evolution of the energy and subsequently discuss the proposed controller.

A. TIME EVOLUTION OF KINEMATIC ENERGY

The kinematic energy E_p of the beam when $U = 0$ can be written as

$$E_p = \int_0^L \left(\frac{1}{2}\hat{M}\dot{y}^2 + \frac{1}{2}EIy''^2 + \hat{M}gy \right) dx \tag{21}$$

The derivative of the energy can be calculated as follows by using (19) and (20) under the assumption that R_i is not a function of x:

$$\dot{E}_p = -E^*I \int_0^L \dot{y}''^2 dx - MU\dot{y}_L^2 + R_s\dot{y}_L + R_i y'_L \dot{y}_L - R_i \int_0^L y'\dot{y}' dx. \tag{22}$$

where $y_L = y(L)$. The first and second terms represent the energy dissipation caused by the viscoelastic term of the beam (Kelvin–Voigt damping effect) and fluid flow (Coriolis term $2MU\dot{y}'$), respectively. The third term represents the ratio of the mechanical work performed by the net force on the nozzle along the $\boldsymbol{e}_{shear}$ direction. The fourth and fifth terms represent the ratio of the mechanical work along the $\boldsymbol{e}_{in}$ direction (explained subsequently).

The first and second terms always dissipate energy because they are non-positive values. The second term, which corresponds to the Coriolis effect, dissipates more energy for a high flow speed. Thus, if we design the control inputs, R_i and R_s for no energy gain, the controller can ensure energy dissipation regardless of the flow speed. Moreover, a high flow speed results in a high damping. This feature differs from that of previous studies. For an ordinal cantilevered pipe without a nozzle, such as in [22], [30], the net force is given as $R_i = -MU^2$ and $R_s = 0$. In this case, the fourth and fifth terms increase as the flow speed increases, which results in an undesired flutter phenomenon.

The fourth and fifth terms represent the ratio of the mechanical work executed by the nozzle along the $\boldsymbol{e}_{in}$ direction. The fourth term itself appears to represent the $\boldsymbol{e}_{in}$ element of the mechanical work ratio caused by the net force of the nozzle unit because it multiplies the $\boldsymbol{e}_{in}$ element of the net force: R_i and $\boldsymbol{e}_{in}$ element of the tip velocity, $y'_L\dot{y}_L$. However, it contains ostensible mechanical work related to the deformation of the beam length. This deformation is attributed to the approximation error of the Euler–Bernoulli beam; thus, this ostensible work should be excluded as the fifth term. This work can be derived by multiplying the length deformation ratio with the net force as follows:

$$R_i \frac{\partial}{\partial t}\left(\int_0^L \sqrt{1+y'^2}dx - L \right) \sim R_i \frac{\partial}{\partial t}\left(\int_0^L \frac{1}{2}y'^2 dx \right). \tag{23}$$

B. PROPOSED CONTROLLER

We propose the controller as follows:

$$\begin{aligned} R_i &= 0 \\ R_s &= K(y_d - y_L) - D\dot{y}_L \end{aligned} \tag{24}$$

where K and D are non-negative gain parameters, and y_d is the desired height of the nozzle unit. This is a PD controller for the height of the nozzle unit. The gains K and D can adjust the responsiveness of the system.

If we define the energy function V as

$$V = E_p + \frac{1}{2}K(y_d - y_L)^2, \tag{25}$$

the time derivative of V can be calculated as follows:

$$\dot{V} = -E^*I \int_0^L \dot{y}''^2 dx - MU\dot{y}_L^2 - D\dot{y}_L^2 \le 0 \tag{26}$$

The proposed simple PD controller can ensure energy dissipation (passivity). Moreover, the effect of the fluid structure interaction (the second term) can be used to improve the speed of energy dissipation. This energy dissipation feature is very useful because the energy function can be a Lyapunov function that ensures system stability. However, we do not discuss the theoretical stability analysis because the proof itself requires further mathematical analysis, which is beyond the scope of this study because of the distributed parameter system [31]. Thus, we numerically evaluate the system stability by linearizing the EQM using the Galerkin method in addition to conducting experiments.

V. DISCRETIZED EQUATION OF MOTION

A. NON-DIMENSIONAL EQM AND CONTROLLER

To reduce the parameters for the simulation, the following non-dimensional quantities and equations are introduced using L and $L^2((M+m)/EI)^{1/2}$ as the reference length and time, respectively.

$$\xi = \frac{x}{L}, \quad \eta = \frac{y}{L}, \quad \tau = \left(\frac{EI}{M+m}\right)^{\frac{1}{2}} \frac{t}{L^2} \tag{27}$$

$$\eta'''' + \alpha\dot{\eta}'''' + [1 + \Gamma_n\delta(\xi - 1)]\ddot{\eta} + \gamma[1 + \Gamma_n\delta(\xi - 1)] + 2\beta^{\frac{1}{2}}u\dot{\eta}' - r_i\eta'' - r_s\delta(\xi - 1) = 0. \tag{28}$$

$$\eta(0) = \eta'(0) = \left(1 + \alpha\frac{\partial}{\partial\tau}\right)\eta''(1) = 0, \quad \left(1 + \alpha\frac{\partial}{\partial\tau}\right)\eta'''(1) = 0 \tag{29}$$

where the other non-dimensional parameters are

$$\alpha = \left[\frac{I}{E(M+m)}\right]^{\frac{1}{2}} \frac{E^*}{L^2}, \quad \beta = \frac{M}{M+m},$$
$$\gamma = \frac{L^3(M+m)}{EI}g, \quad u = \left(\frac{M}{EI}\right)^{\frac{1}{2}} LU, \quad r_i = \frac{L^2R_i}{EI},$$
$$r_s = \frac{L^2R_s}{EI}, \quad \Gamma_n = \frac{m_n}{(M+m)L}$$

Therefore, the non-dimensional controller can be expressed as

$$r_i = 0, \quad r_s = k(\eta_d - \eta_L) - d\dot{\eta}_L, \tag{30}$$

where

$$k = \frac{L^3 K}{EI}, \quad d = \left[\frac{1}{(M+m)EI}\right]^{\frac{1}{2}} LD, \quad \eta_d = \frac{y_d}{L}.$$

B. LINEARIZATION BY GALERKIN DISCRETIZATION

The standard Galerkin technique [11] is applied to transform the coupled partial differential equations into linearized ordinary differential equations. The comparison functions are set as the eigenfunctions of the normal cantilever beam $\eta'''' + \ddot{\eta} = 0$ as

$$\begin{aligned} \phi_i(\xi) &= \cosh(\lambda_i \xi) - \cos(\lambda_i \xi) - \sigma_i \left[\sinh(\lambda_i \xi) - \sin(\lambda_i \xi)\right] \\ \sigma_i &= \frac{\sinh \lambda_i - \sin \lambda_i}{\cosh \lambda_i + \cos \lambda_i} \end{aligned} \tag{31}$$

where λ_i is the solution of $1 + \cosh \lambda_i \cos \lambda_i = 0$.

The solution of EQM(28) is approximated as the summation of N eigenfunctions as follows:

$$w_N = \sum_{i=1}^{N} \phi_i(\xi) q_i(t). \tag{32}$$

Here, q_i fulfils the following condition:

$$\int_0^1 \epsilon[w_N] \phi_i(\xi) d\xi = 0 \tag{33}$$

where $\epsilon[w_N]$ represents the error of EQM(28) when $\eta = w_N$ is substituted into (28).

Consequently, the following Nth linearlized equations are derived:

$$0 = \boldsymbol{M}\ddot{\boldsymbol{q}} + \boldsymbol{C}\dot{\boldsymbol{q}} + \boldsymbol{K}\boldsymbol{q} + \boldsymbol{g} \tag{34}$$

where $\boldsymbol{q} = [q_1\, q_2\, \cdots\, q_N]^T$, and the elements of $\boldsymbol{M}, \boldsymbol{C}, \boldsymbol{K}, \boldsymbol{g}$ are as follows:

$$\begin{aligned} M_{ij} &= \delta_{ij} + \Gamma_n \phi_i(1) \phi_j(1), \\ C_{ij} &= \alpha \lambda_j^4 \delta_{ij} + 2\beta^{\frac{1}{2}} u \int_0^1 \phi_i \phi_j' d\xi + d\phi_i(1)\phi_j(1), \\ K_{ij} &= \lambda_j^4 \delta_{ij} + k\phi_i(1)\phi_j(1), \\ g_i &= \int_0^1 \gamma \phi_i d\xi + \gamma \Gamma_n \phi_i(1) - k\eta_d \phi_i(1), \end{aligned}$$

where $i, j \in [1,\ N]$.

C. LINEARIZED DYNAMICS

If the inverse exists for the matrix $\boldsymbol{M}$, the linearized EQM can be rewritten as follows (the inverse matrix always exists in the following simulations, although it could not be proved):

$$\frac{d\boldsymbol{p}}{d\tau} = \boldsymbol{A}\boldsymbol{p} + \boldsymbol{b}, \tag{35}$$

where $\boldsymbol{p} = [\boldsymbol{q}^T\, \dot{\boldsymbol{q}}^T]^T$, and

$$\boldsymbol{A} = \begin{bmatrix} \boldsymbol{0}_{N\times N} & \boldsymbol{E} \\ -\boldsymbol{M}^{-1}\boldsymbol{K} & -\boldsymbol{M}^{-1}\boldsymbol{C} \end{bmatrix}, \quad \boldsymbol{b} = \begin{bmatrix} \boldsymbol{0}_{N\times 1} \\ -\boldsymbol{M}^{-1}\boldsymbol{g} \end{bmatrix}, \tag{36}$$

where $\boldsymbol{E} \in \mathbb{R}^{N\times N}$ is an identity matrix. The equilibrium point $\boldsymbol{q}^*$ can be calculated as $\boldsymbol{q}^* = -\boldsymbol{K}^{-1}\boldsymbol{g}$, and the linear stability can be evaluated using the eigenvalues $\boldsymbol{\Lambda}$ of $\boldsymbol{A}$. We note that the desired height η_d and gravity term γ only appear in $\boldsymbol{g}$, which affects the equilibrium point $\boldsymbol{q}^*$ and not linear stability. Therefore, the next section numerically investigates the stability by setting η_d and γ to zero.

VI. SIMULATION

A. STABILITY DUE TO THE DAMPING EFFECT OF FLOWING FLUID

We conduct a simulation to verify the stabilization owing to the damping effect of the fluid. The damping and gravity terms of the body are assumed to be zero ($\alpha = 0,\ \gamma = 0$), and the three weight ratios of water to the body (β) are set according to the literature [11] ($\beta = 0.2,\ 0.295,\ 0.5$). The discretization order is set to $N = 10$ based on [11]. Focusing on the effect of the flow speed, the control parameter was set to $k = d = \eta_d = 0$. We investigate the change in the linear stability at $\boldsymbol{q}^* = \boldsymbol{0}$ against flow speed u. Note that if the tip water channel is opened (no nozzle), the pipe motion becomes unstable when the flow speed exceeds $u_{cf} = 5.60,\ 8.20$, and 9.33 for $\beta = 0.2,\ 0.295$, and 0.5, respectively, [11].

The response of the eigenvalue $\boldsymbol{\Lambda}$ against flow speed u is shown in Figs.4A, B, and C, which correspond to the values of $\beta = 0.2,\ 0.295$, and 0.5, respectively. The horizontal axis represents the imaginary part of each eigenvalue, and the vertical axis represents the negative real part of the eigenvalue; crossing the y-axis downward indicates destabilization of the corresponding mode. The value of u is indicated by the color of each point. Similarly, Figures 4A2, B2, and C2 exhibit a change in the maximum real part of the eigenvalue with respect to u. Instability occurs when the eigenvalue becomes larger than zero.

The results indicate that the flowing fluid does not cause instability but acts as a damping term for the system and improves the stability of the higher modes. For Figs. 4A2, B2, and C2, the maximum real part of the eigenvalues decreases monotonically as the flow speed increases from zero. In contrast, when the flow speed exceeds a certain value, the maximum real part of the eigenvalues approaches zero (not greater than zero). In this case, the eigenvalue of the first-order mode tends to approach the zero eigenvalue along the real axis, as shown in Figs. 4A1, B1, and C1. This means that the first-order mode is overdamped. In contrast, the real part of the eigenvalues of the second-order and higher modes reduces uniformly with an increase in the flow speed, indicating that the fluid damping effect improves the stability of these modes. This improvement in the stability of higher-order modes is more prominent when the fluid fraction is larger (i.e., β is larger).

B. STABILITY DUE TO THE CONTROL PARAMETERS

We examine the effect of the control parameters k and d on the stability under the same configuration as in the previous

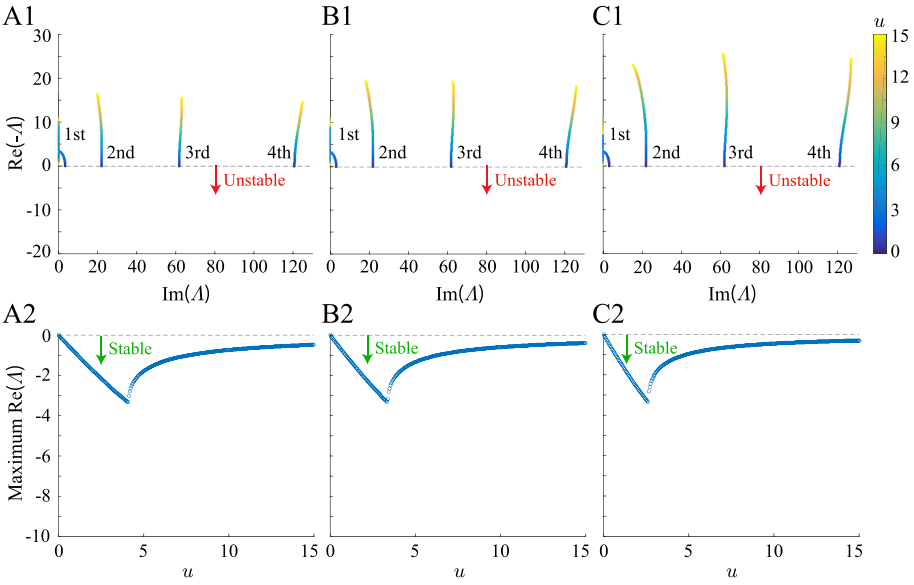

FIGURE 4. Responses of eigenvalues Λ depending on fluid velocity u with the nozzle control ($k = d = 0$) for $\beta = 0.2$ (A1), 0.295 (B1), and 0.5 (C1). The responses of the maximum real part of eigenvalues Λ depending on the fluid velocity u with the nozzle control ($k = d = 0$) for $\beta = 0.2$ (A2), 0.295 (B2), and 0.5 (C2).

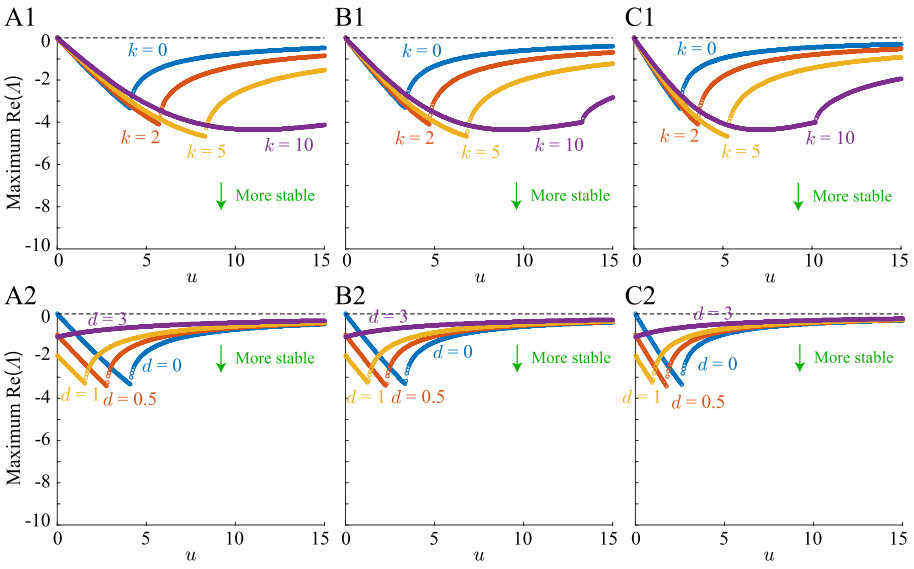

FIGURE 5. Responses of maximum real part of eigenvalues Λ for various P and D control gains (k and d) for $\beta = 0.2$ (A), 0.295 (B), and 0.5 (C).

simulation. The maximum real parts of the eigenvalues for various P gains k are shown in Figs. 5A1, B1, and C1 ($d = 0$). Similar graphs for various D gains, d, are shown in Figs. 5A2, B2, and C2 ($k = 0$). The figures A, B, and C correspond to $\beta = 0.2,\ 0.295,$ and 0.5.

For all β, we confirm that an increase in the P gain k improves the stability at a high flow speed. This suggests that increasing the P gain prevents over-damping at high flow speeds. In contrast, increasing the D gain d deteriorates the stability for a high flow speed. The increase in the D gain causes an over-damping situation. From these results, we found that the stability of the system can be improved by appropriately setting the control parameters.

VII. EXPERIMENTS

A. DEVELOPED ROBOT

The robot developed for this experiment is shown in Fig. 6. The robot consists of a nozzle unit at the tip and a 2.4 m long body. The body part consists of a PVC pipe (VU40) with a water hose (inner diameter: 25 mm) fixed inside.

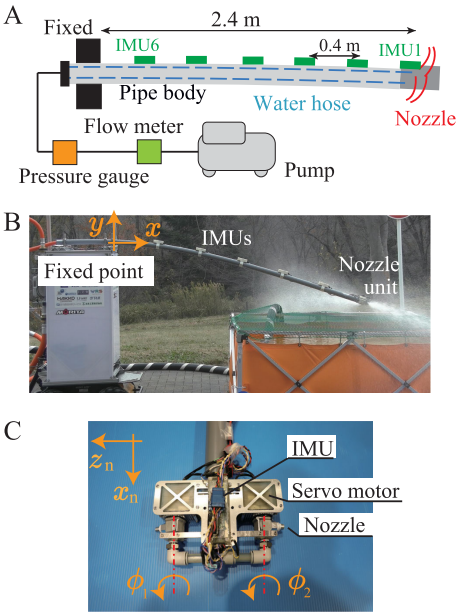

FIGURE 6. Developed testbed for experiments: Overview of the experimental system(A), side view of the robot(B), and structure of nozzle unit(C).

TABLE 1. Test bed physical parameters.

Parameters	Variables	Values
Unit mass of pipe [kg/m]	m	1.11
Unit mass of water [kg/m]	M	0.491
Mass of nozzle [kg]	m_n	1.23
Length of pipe [m]	L	2.40
Second moment of area [m^4]	I	7.66×10^{-8}
Young's modulus [Pa]	E	2.93×10^{9}
Kelvin–Voigt coefficient [sPa]	E^*	3.56×10^{7}
Gravity acceleration [m/s^2]	g	9.80

Multiple inertial measurement units (IMUs) are mounted on the outside of the pipe. The root of the pipe is fixed. The root of the water hose is connected to a flowmeter (*Keyence*, FD-R50) and a pressure gauge (*Nagano Keiki*, GC31). The detailed physical parameters of the robot are listed in Table 1, and the non-dimensional parameters are listed in Table 2. To install the proposed controller on the robot, the position and velocity of the nozzle unit should be measured, and the nozzle unit should realize a normal net force.

To estimate the position and velocity of the nozzle unit, the pipe was approximated as a connection of seven rigid links with six joints (0.2 m long links at the end and tip, 0.4 m long links for others) whose attitudes and angular velocities are measured by the IMUs. Six IMUs (*TDK*, ICM-20948) were mounted on the nozzle unit and pipe at 0.4 m intervals. Each IMU measured the angular velocity and acceleration at 1 kHz,

TABLE 2. Nondimensional parameters of the test bed.

α	0.0249	γ	0.968
β	0.306	Γ	0.320

which were converted to attitude using the Madgwick filter [32] at 100 Hz. We note that the approximation error of this discrete position estimation is affordable for this experiment. The circular curve with a curvature of 0.3 /m (which is estimated from the attitudes of IMUs) can be approximated with a head position error less than 0.003 m, which is almost 30 times smaller than the given disturbance.

The structure and coordinate system of the nozzle unit are shown in Fig. 6C. The nozzle unit consists of two nozzles that can rotate around one axis (x_n axis), and each nozzle has a diameter of 7 mm. The rotation angles of the nozzles are represented by ϕ_1 and ϕ_2. The angle is zero when each nozzle faces directly down (in the $-y_n$ direction). The position-controlled servomotors (*ROBOTIS*, Dynamixel MX28) control the angles ϕ_1 and ϕ_2. Owing to geometric constraints, we set $-\pi < \phi_1 \leq 0$ and $0 \leq \phi_2 \leq \pi$. These constraints were always fulfilled during the experiment.

The nozzle angles can be determined to realize the normal force R_s when the roll posture of the nozzle unit is given as θ_{rn},

$$\phi_1 = -\phi_a - \theta_{rn} \tag{37}$$

$$\phi_2 = \phi_a - \theta_{rn} \tag{38}$$

where $\phi_a = \arccos\left(\frac{R_s}{2F_n}\right)$, and F_n is the reaction force of each nozzle. The reaction force F_n is determined by $F_n = 28.3p$, where p is the relative pressure (derived from a preliminary experiment). The net force R_s (control input) is realized at 100 Hz by measuring p and commanding $\phi_{1,2}$ at 100 Hz.

B. VALIDATION OF THE FLUID DAMPING EFFECT

We investigated the disturbance response for various flow speeds with control gains $K = D = 0$ to verify the fluid damping effect. For each flow speed, the root pressure (flow speed) was fixed, six initial disturbances were applied to the tip using a rod, and the time responses of the tip position were measured. The root pressure was changed for all seven patterns. Examples of the measured time responses to the disturbances are shown in Fig. 7A (see supplementary video). We found that the convergence time decreased as the flow speed increased, which exhibited a damping effect.

To investigate this tendency quantitatively, we define the following four indices for the time responses of the head height against disturbance.

(a) Settling time (the time when the deviation is less than 15% of the initial error)
(b) Rise time (the time when the deviation changes from 90% to 10% of the initial error)
(c) Overshoot
(d) Equilibrium position (mean value of y_L for 10 s without a disturbance)

In addition, we numerically calculate the time response of the head height and the above four indices to compare and validate the simulation. We numerically solve the linearized equation (35) with the parameters in Table 2. The initial state

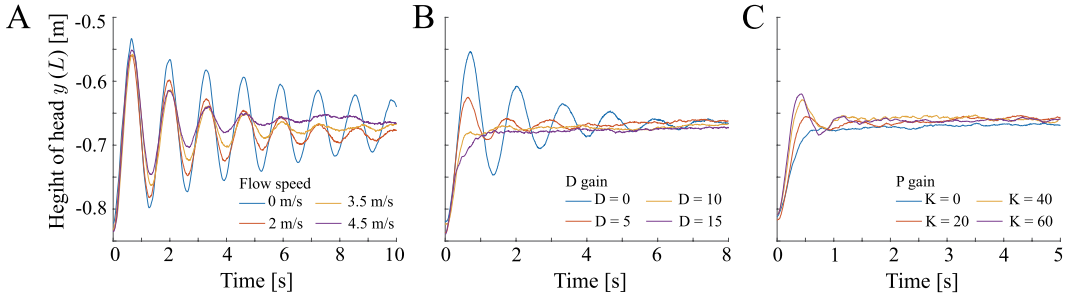

FIGURE 7. Time responses of the head heights against disturbances for various flow speeds(A), D control gains(B), and P control gains(C).

as a disturbance is given as the equilibrium shape when the head is applied with a 10 N downward external force.

The responses of these four indices against the flow speed U are shown in Figs. 8A(a)–(d). The simulation results are shown in the same figures. The results indicated that the settling time decreased and the stability improved as the flow speed increased. This trend is also consistent with the simulation results. The rise time was almost constant, similar to the simulation results. The overshoot tends to decrease with the flow velocity except at the point where $U = 0$, which is also consistent with the simulation results. These results show that the stability can be improved according to the flow speed, and that the experimental results are in good agreement with those of the simulation.

In contrast, the equilibrium height was significantly different from the simulation results. This is because of the initial bending tendency in the pipe. However, the equilibrium height is almost constant with respect to the flow speed, which is consistent with the simulation results. Moreover, the overshoot value at $U = 0$ was significantly different from that of the simulation. This may be attributed to the influence of the internal fluid movement according to the pipe oscillation in the experiment. We note that the settling time in the simulation decreased stepwise because the time response of $y(L)$ oscillates, as shown in Fig. 7A, meaning that the settling timing may jump by one wavelength when U changes.

C. RESULT FOR D GAIN CHANGE

To validate the adjustability of the responsiveness using the D gain of the proposed controller, we measured the disturbance response for various D gains, while the root pressure and controller P gain were fixed at 0.6 MPa (flow velocity of 3.66 m/s) and $K = 0$, respectively. The disturbance was created six times at each D gain, and the D gain was varied for seven patterns. Examples of the time response to the disturbances are shown in Fig. 7B (see supplementary video). As the D gain increased, the convergence time decreased, and the overshoot tended to disappear. At $D = 15$, we observe an over-damping case.

For quantitative analysis, we introduced the four indices discussed in the previous section. The responses of these four indices to D are shown in Figs. 8B(a)–(d). The simulation results for identical cases are illustrated in the same figure. To evaluate the motor response delay in the experiment, we also conducted simulations where first-order filters with time constants of 0.03 and 0.07 s are applied to the output of the control equation (24).

The settling time tends to decrease and then increases slightly as the D gain increases, indicating that the stability can be improved by selecting an appropriate gain. This trend is in good agreement with the simulations. Moreover, the rise time tends to increase with the D gain, which is consistent with the simulation results. The overshoot tended to decrease with the D gain, which is also consistent with the simulation results. These results show that the stability and responsiveness of the controller can be adjusted according to the D gain.

In contrast, the equilibrium height is significantly different from the simulation, which is speculated to be due to the same reason as in the previous section. In addition, for the rise time, the experimental and simulation values differed significantly for a high D gain. We believe that this is because the time delay in the motor response becomes significant when the D gain increases. In fact, when a first-order filter was added to the simulation, the tendency was contiguous with the experimental results. However, there is still a considerable error in the rise time. This is probably because the nozzle angles do not correspond to the commanded values due to backlash.

D. RESULT FOR P GAIN CHANGE

To validate the adjustability of the responsiveness using the P gain, we measured the disturbance responses for different P gains K while the root pressure, controller D gain, and desired position were fixed at approximately 0.6 MPa (flow velocity of 3.72 m/s), $D = 0$, and $y_d = -0.66$, respectively. The disturbance was introduced six times at each P gain, and the P gain was changed for eight patterns. Examples of the time response to the disturbances are shown in Fig. 7C (see supplementary video). As the P gain increased, the rise time decreased, and the overshoot tended to increase.

For quantitative analysis, we introduced the four indices described in the previous section. The responses of these four indices to K are shown in Figs. 8C(a)–(d). The simulation results for the same cases are shown in the same figure.

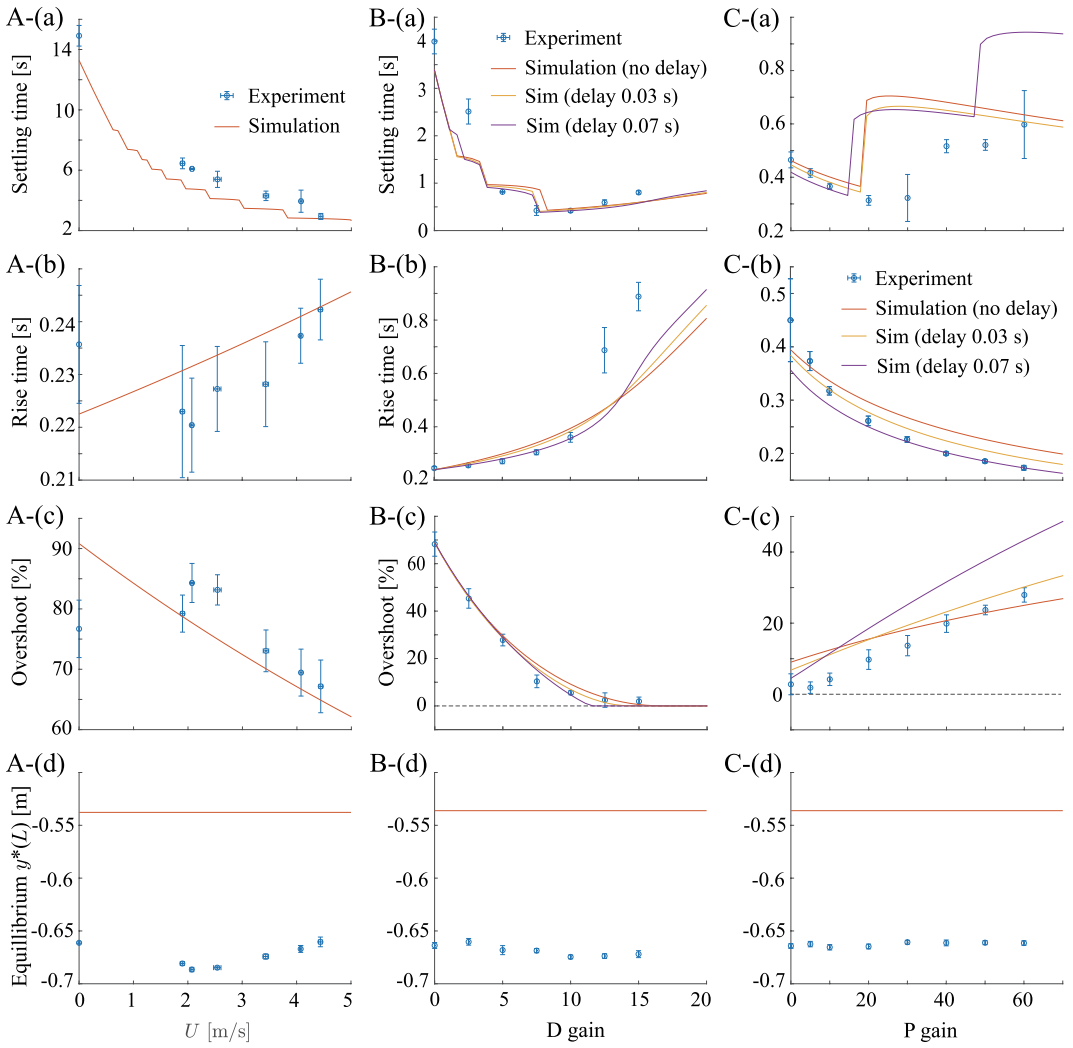

FIGURE 8. Responses of four indexes ((a)Settling time, (b)Rise time, (c)Overshoot, and (d)Equilibrium height of tip) against various flow speeds(A), D control gains(B), and P control gains(C). Points and lines represent the measured values and simulation results, respectively.

To evaluate the delay of the motor response in the experiment, we also conducted simulations with first-order filters, as in the previous section. Note that we set $y_d = -0.54$ in the simulation, so as not to change the simulation's equilibrium point.

The settling time increased with the P gain in a stepwise manner, which was also observed in the simulations. In addition, the rise time decreases, and the overshoot increases with the P gain, which is consistent with the simulation results. These results show that the responsiveness can be adjusted according to the P gain in this controller.

In contrast, the equilibrium height differs significantly from that of the simulation, but this is speculated to be due to the same reason as in the previous sections. For the convergence time, the location of the step was different for the experiment and simulation. This may be attributed to the nozzle backlash, which prevents the commanded force from realization and lowers the P gain in the experiment. However, the overall tendency for the convergence time to increase is consistent.

VIII. CONCLUSION

In this study, we proposed a stabilized controller (vertical position controller) for a jet-actuated two-dimensional cantilevered pipe with a nozzle unit at the tip using the damping effect of the internal flowing fluid, and verified the controller with a real robot. We derived a model based on several assumptions. The time evolution characteristics of the model energy function were analyzed, and a controller was proposed that can constantly decrease the energy function. The proposed controller was verified using simulations, and it was confirmed that the system was stable regardless of the flow velocity. In particular, the fluid effect contributed to suppressing higher-order mode oscillations. Moreover, we confirmed that the stability could be improved by tuning the gains of the proposed controller. Finally, the proposed controller and

simulations were verified through experiments. The experiments proved that the vibrations could be damped by the fluid effect and that the stability and responsiveness of the system could be improved by tuning the gains of the controller.

The results provide significant suggestions and insights for future control strategies of jet-actuated continuum robots. For example, the proposed controller can stabilize the higher-order modes by utilizing fluid effects, even though the number of control inputs is small. This control strategy, using the damping property of the flowing fluid, would be very useful for continuum robots, because they are also distributed parameter systems with a limited number of actuators, such as the DFF controlled by the discrete nozzle units [6]–[8].

In the future, we aim to improve the model to handle significant deformations, for applications in jet-actuated continuum robots, such as DFF. Moreover, we aim to develop a controller for robots, based on the results of this study. Furthermore, we plan to create a three-dimensional model. Additionally, the theoretical proof of stability, which was not discussed in this paper, should be an area of focus.

REFERENCES

[1] Y. Yamauchi, Y. Ambe, M. Konyo, K. Tadakuma, and S. Tadokoro, "Passive orientation control of nozzle unit with multiple water jets to expand the net force direction range for aerial hose-type robots," *IEEE Robot. Autom. Lett.*, vol. 6, no. 3, pp. 5634–5641, Jul. 2021.

[2] J. A. S. Rico, G. Endo, S. Hirose, and H. Yamada, "Development of an actuation system based on water jet propulsion for a slim long-reach robot," *Robomech J.*, vol. 4, no. 1, Mar. 2017, doi: 10.1186/s40648-017-0076-4.

[3] J. Liu, L. Yin, J. H. Chandler, X. Chen, P. Valdastri, and S. Zuo, "A dual-bending endoscope with shape-lockable hydraulic actuation and water-jet propulsion for gastrointestinal tract screening," *Int. J. Med. Robot. Comput. Assist. Surgery*, vol. 17, no. 1, pp. 1–13, Feb. 2021.

[4] D. Eberl and F. Majdic, "Hose manipulation with jet forces," *Ventil*, vol. 21, no. 4, pp. 286–290, 2015.

[5] A. Ishii, Y. Ambe, Y. Yamauchi, H. Ando, M. Konyo, K. Tadakuma, and S. Tadokoro, "Design and development of biaxial active nozzle with flexible flow channel for air floating active scope camera," in *Proc. IEEE/RSJ Int. Conf. Intell. Robots Syst. (IROS)*, Oct. 2018, pp. 442–449.

[6] H. Ando, Y. Ambe, A. Ishii, M. Konyo, K. Tadakuma, S. Maruyama, and S. Tadokoro, "Aerial hose type robot by water jet for fire fighting," *IEEE Robot. Autom. Lett.*, vol. 3, no. 2, pp. 1128–1135, Apr. 2018.

[7] T. Yamaguchi, Y. Ambe, H. Ando, M. Konyo, K. Tadakuma, S. Maruyama, and S. Tadokoro, "A mechanical approach to suppress the oscillation of a long continuum robot flying with water jets," *IEEE Robot. Autom. Lett.*, vol. 4, no. 4, pp. 4346–4353, Oct. 2019.

[8] H. Ando, Y. Ambe, T. Yamaguchi, Y. Yamauchi, M. Konyo, K. Tadakuma, S. Maruyama, and S. Tadokoro, "Fire extinguishment using a 4 m long flying-hose-type robot with multiple water-jet nozzles," *Adv. Robot.*, vol. 34, no. 11, pp. 700–714, Jun. 2020, doi: 10.1080/01691864.2020.1769723.

[9] D.-H. Lee, T. Huynh, Y.-B. Kim, and C. Soumayya, "Motion control system design for a flying-type firefighting system with water jet actuators," *Actuators*, vol. 10, no. 10, p. 275, Oct. 2021. [Online]. Available: https://www.mdpi.com/2076-0825/10/10/275

[10] R. A. Ibrahim, "Overview of mechanics of pipes conveying fluids—Part I: Fundamental studies," *J. Pressure Vessel Technol.*, vol. 132, no. 3, pp. 03001–034001, Jun. 2010.

[11] M. P. Païdoussis, *Fluid-Structure Interactions: Slender Structures and Axial Flow*, vol. 1, 2nd ed. New York, NY, USA: Academic, 2014.

[12] M. P. Païdoussis and C. Semler, "Non-linear dynamics of a fluid-conveying cantilevered pipe with a small mass attached at the free end," *Int. J. Non-Linear Mech.*, vol. 33, no. 1, pp. 15–32, Jan. 1998. [Online]. Available: https://www.sciencedirect.com/science/article/pii/S0020746297000024

[13] K. Yamashita, J. Ajiro, A. Motoki, Y. Hirose, H. Yabuno, and M. Yoshizawa, "Nonlinear stabilities of lateral virbrations of a pipe conveying fluid (in case of a pipe with a spring supported end)," *Trans. Jpn. Soc. Mech. Eng. C*, vol. 76, no. 762, pp. 236–243, 2010.

[14] J. D. Jin and G. S. Zou, "Bifurcations and chaotic motions in the autonomous system of a restrained pipe conveying fluid," *J. Sound Vibrat.*, vol. 260, no. 5, pp. 783–805, Mar. 2003. [Online]. Available: https://www.sciencedirect.com/science/article/pii/S0022460X02009823

[15] Y. Wang, L. Wang, Q. Ni, H. Dai, H. Yan, and Y. Luo, "Non-planar responses of cantilevered pipes conveying fluid with intermediate motion constraints," *Nonlinear Dyn.*, vol. 93, no. 2, pp. 505–524, Jul. 2018.

[16] B. Rong, K. Lu, X.-T. Rui, X.-J. Ni, L. Tao, and G.-P. Wang, "Nonlinear dynamics analysis of pipe conveying fluid by Riccati absolute nodal coordinate transfer matrix method," *Nonlinear Dyn.*, vol. 92, no. 2, pp. 699–708, Apr. 2018.

[17] W. Chen, H. Dai, Q. Jia, and L. Wang, "Geometrically exact equation of motion for large-amplitude oscillation of cantilevered pipe conveying fluid," *Nonlinear Dyn.*, vol. 98, no. 3, pp. 2097–2114, Nov. 2019.

[18] W. Chen, H. Dai, and L. Wang, "Three-dimensional dynamical model for cantilevered pipes conveying fluid under large deformation," *J. Fluids Struct.*, vol. 105, Aug. 2021, Art. no. 103329. [Online]. Available: https://www.sciencedirect.com/science/article/pii/S0889974621001122

[19] K. Zhou, Q. Ni, W. Chen, H. L. Dai, P. Hagedorn, and L. Wang, "Static equilibrium configuration and nonlinear dynamics of slightly curved cantilevered pipe conveying fluid," *J. Sound Vibrat.*, vol. 490, Jan. 2021, Art. no. 115711. [Online]. Available: https://www.sciencedirect.com/science/article/pii/S0022460X20305411

[20] M. P. Paidoussis and C. Sundararajan, "Parametric and combination resonances of a pipe conveying pulsating fluid," *J. Appl. Mech.*, vol. 42, no. 4, pp. 780–784, Dec. 1975.

[21] A. R. Askarian, H. Haddadpour, R. D. Firouz-Abadi, and H. Abtahi, "Nonlinear dynamics of extensible viscoelastic cantilevered pipes conveying pulsatile flow with an end nozzle," *Int. J. Non-Linear Mech.*, vol. 91, pp. 22–35, May 2017. [Online]. Available: https://www.sciencedirect.com/science/article/pii/S0020746217300860

[22] Y. Sugiyama, T. Katayama, E. Kanki, K. Nishino, and B. Akesson, "Stabilization of cantilevered flexible structures by means of an internal flowing fluid," *J. Fluids Struct.*, vol. 10, no. 6, pp. 653–661, 1996. [Online]. Available: https://www.sciencedirect.com/science/article/pii/S0889974696900432

[23] H. Doki, K. Hiramoto, and R. E. Skelton, "Active control of cantilevered pipes conveying fluid with constraints on input energy," *J. Fluids Struct.*, vol. 12, no. 5, pp. 615–628, Jul. 1998.

[24] D. Pisarski, R. Konowrocki, and T. Szmidt, "Dynamics and optimal control of an electromagnetically actuated cantilever pipe conveying fluid," *J. Sound Vibrat.*, vol. 432, pp. 420–436, Oct. 2018. [Online]. Available: https://www.sciencedirect.com/science/article/pii/S0022460X18304073 s

[25] T.-Z. Yang, X.-D. Yang, Y. Li, and B. Fang, "Passive and adaptive vibration suppression of pipes conveying fluid with variable velocity," *J. Vibrat. Control*, vol. 20, no. 9, pp. 1293–1300, Jul. 2014.

[26] K. Zhou, F. R. Xiong, N. B. Jiang, H. L. Dai, H. Yan, L. Wang, and Q. Ni, "Nonlinear vibration control of a cantilevered fluid-conveying pipe using the idea of nonlinear energy sink," *Nonlinear Dyn.*, vol. 95, no. 2, pp. 1435–1456, Jan. 2019.

[27] Z. Liu, K. Zhou, L. Wang, T. Jiang, and H. Dai, "Dynamical stability of cantilevered pipe conveying fluid in the presence of linear dynamic vibration absorber," *J. Comput. Appl. Mech.*, vol. 50, no. 1, pp. 182–190, 2019. [Online]. Available: https://jcamech.ut.ac.ir/article_69971.html

[28] B. Yu, H. Yabuno, and K. Yamashita, "Stabilization of a flexible pipe conveying fluid with an active boundary control method," *J. Vibrat. Control*, vol. 26, nos. 19–20, pp. 1824–1834, Oct. 2020.

[29] D. Borglund, "Active nozzle control and integrated design optimization of a beam subject to fluid-dynamic forces," *J. Fluids Struct.*, vol. 13, no. 2, pp. 269–287, 1999. [Online]. Available: http://www.sciencedirect.com/science/article/pii/S0889974698901967

[30] M. P. Païdoussis and N. T. Issid, "Dynamic stability of pipes conveying fluid," *J. Sound Vibrat.*, vol. 33, no. 3, pp. 267–294, Apr. 1974. [Online]. Available: http://www.sciencedirect.com/science/article/pii/S0022460X74800027

[31] T. Endo and H. Kawasaki, "Bending moment-based force control of flexible arm under gravity," *Mechanism Mach. Theory*, vol. 79, pp. 217–229, Sep. 2014. [Online]. Available: https://www.sciencedirect.com/science/article/pii/S0094114X14001207

[32] S. O. H. Madgwick, A. J. L. Harrison, and R. Vaidyanathan, "Estimation of IMU and MARG orientation using a gradient descent algorithm," in *Proc. IEEE Int. Conf. Rehabil. Robot.*, Jun. 2011, pp. 1–7.

YUICHI AMBE (Member, IEEE) received the Ph.D. degree in engineering from Kyoto University, Kyoto, Japan, in 2017.

From 2018 to 2020, he was an Assistant Professor at the Graduate School of Engineering, Tohoku University, Japan. Since 2021, he has been an Assistant Professor at the Tough Cyberphysical AI Research Center, Tohoku University. His research interests include the design and control of continuum robots, jet-actuated aerial robots, legged robots, and rescue robots.

YU YAMAUCHI (Graduate Student Member, IEEE) received the M.S. degree in information science from Tohoku University, Miyagi, Japan, in 2019, where he is currently pursuing the Ph.D. degree in the design and control of jet-actuated continuum robots.

His research interests include the design and control of continuum robots.

MASASHI KONYO (Member, IEEE) received the B.S., M.S., and Ph.D. degrees in engineering from Kobe University, Hyogo, Japan, in 1999, 2001, and 2004, respectively.

He is currently an Associate Professor at the Graduate School of Information Sciences, Tohoku University. His research interests include haptic interfaces, rescue robotics, and new actuators. He was a recipient of the Young Scientists Prize, the Commendation for Science and Technology by MEXT in 2015, the Best Paper Awards of the *Journals of Robotics and Mechatronics* in 2010, Advanced Robotics in 2016, the Best Poster Awards of the World Haptics Conference in 2007, and 2013, and the Best Hands-on Demo Award at the Euro-Haptics 2008 and Haptics Symposium 2014.

KENJIRO TADAKUMA (Member, IEEE) received the Ph.D. degree in mechanical and aerospace engineering from the Tokyo Institute of Technology, Tokyo, Japan in 2007.

He is currently an Associate Professor at the Graduate School of Information Sciences, Tohoku University. His research interests include mechanisms, omnidirectional mobile robots, and rescue robots.

Dr. Tadakuma was a recipient of the Young Scientists' Prize for the Commendation of Science and Technology by the Minister of Education, Culture, Sports, Science and Technology (MEXT) in 2011.

SATOSHI TADOKORO (Fellow, IEEE) graduated from The University of Tokyo, in 1984.

From 1993 to 2005, he was an Associate Professor at Kobe University. Since 2002, he has been the President of the International Rescue System Institute. Since 2005, he has been a Professor at Tohoku University. From 2012 to 2014, he was the Vice/Deputy Dean of the Graduate School of Information Sciences. From 2016 to 2017, he was the President of the IEEE Robotics and Automation Society. Since 2019, he has been the Director of the Tough Cyberphysical AI Research Center, Tohoku University. He served as a Program Manager of the MEXT DDT Project on Rescue Robotics from 2002 to 2007, and was a Project Manager of the Japan Cabinet Office ImPACT Tough Robotics Challenge Project on Disaster Robotics, from 2014 to 2019, with 62 international PIs and 300 researchers who created the Cyber Rescue Canine, Dragon Firefighter, etc. His research team at Tohoku University has developed various rescue robots, of which Quince and Active Scope Camera are widely recognized for their contribution to disaster response, including missions in the Fukushima-Daiichi NPP nuclear reactor buildings. He is a RSJ Fellow, JSME Fellow, and SICE Fellow.